Majorana Kramers Pairs in Higher-Order Topological Insulators

Chen-Hsuan Hsu,[1] Peter Stano,[1,2,3] Jelena Klinovaja,[1,4] and Daniel Loss[1,4]
[1]*RIKEN Center for Emergent Matter Science (CEMS), Wako, Saitama 351-0198, Japan*
[2]*Department of Applied Physics, School of Engineering, University of Tokyo, 7-3-1 Hongo, Bunkyo-ku, Tokyo 113-8656, Japan*
[3]*Institute of Physics, Slovak Academy of Sciences, 845 11 Bratislava, Slovakia*
[4]*Department of Physics, University of Basel, Klingelbergstrasse 82, CH-4056 Basel, Switzerland*

(Received 30 May 2018; revised manuscript received 24 August 2018; published 6 November 2018)

We propose a tune-free scheme to realize Kramers pairs of Majorana bound states in recently discovered higher-order topological insulators (HOTIs). We show that, by bringing two hinges of a HOTI into the proximity of an *s*-wave superconductor, the competition between local and crossed Andreev pairing leads to the formation of Majorana Kramers pairs, when the latter pairing dominates over the former. We demonstrate that such a topological superconductivity is stabilized by moderate electron-electron interactions. The proposed setup avoids the application of a magnetic field or local voltage gates, and requires weaker interactions compared with nonhelical nanowires.

DOI: 10.1103/PhysRevLett.121.196801

Majorana bound states (MBSs), with topological quantum computation prospects, have gained much attention recently [1–31]. However, the prototypical realizations based on proximity-induced superconductivity and either semiconducting nanowires with strong spin-orbit interactions [32–44], or topological insulators (TIs) [45,46] require an external magnetic field, detrimental to superconductivity and MBSs themselves. It might also be noted that buried Dirac points are common in two- or three-dimensional TIs (2DTIs/3DTIs) [47–51], impeding the realization of MBSs in TI-superconductor heterostructures using magnetic fields [47].

Platforms without magnetic fields are therefore searched for [52–58], examples including helical spin textures [59–66] and crossed Andreev pairings in double nanowires or 2DTI edge channels [67–73]. In the former, the spin texture arises through indirect coupling mediated by itinerant carriers. The superconducting gap reduces it, leading to a tradeoff between the operation temperature (set by the indirect coupling) and the MBS localization length (set by the superconducting gap). On the other hand, the latter setup requires fine-tuned chemical potentials in two isolated one-dimensional channels. These difficulties motivate us to seek a new scheme to avoid fine-tuning.

Here we propose such a scheme, exploiting the recently discovered higher-order topological insulators (HOTIs) [74–82]. Specifically, we focus on 3D helical second-order TIs. In contrast to the gapless surface states in their first-order counterparts [6,7,83–86], these HOTIs host helical hinge states, in which opposite spins move in opposite directions, akin to the spin-momentum locked edge channels in 2DTIs [87–93]. There is compelling experimental evidence for the topological hinge states in Bi(111) nanowires and bilayers [80,94,95].

Our scheme exploits *s*-wave superconductivity-proximitized helical hinges of a HOTI. Two types of pairings arise, a local (standard) and a nonlocal (crossed Andreev) one. We first demonstrate that Majorana Kramers pairs (MKPs) emerge when the crossed Andreev pairing dominates. This regime, however, does not arise in a noninteracting system. Nevertheless, we show that rather weak electron-electron interactions are sufficient to push the system into a regime where the crossed Andreev pairing dominates. We therefore predict that MKPs typically appear at the ends of a HOTI nanowire.

To elucidate an essential feature, consider that two parallel hinges of a helical HOTI are in contact with an *s*-wave superconductor. Cooper pairs can tunnel into the hinges through two processes. The local (nonlocal) pairing process corresponds to the two partners of a Cooper pair tunneling into the same (different) hinge(s). We denote the configuration as parahelical (orthohelical), when the helicities of the two hinges are the same (opposite). For example, in the parahelical setup a spin-down electron in the two hinges propagates in the same direction, whereas in the orthohelical setup they move in opposite directions. The momentum conservation imposes selection rules: the chemical potentials of the two hinges have to be the same (opposite) for the parahelical (orthohelical) setup [68] to allow for a crossed Andreev pairing. Since the conducting hinges of a HOTI are all connected, their chemical potentials are identical without applying local voltage gates, a substantial advantage.

Setup.—As a concrete example, we consider the recently discovered HOTI material, a bismuth crystal grown along the (111) axis [96], which hosts helical hinge states [80], as drawn in Fig. 1. Since the helicities of any two parallel hinges on the same lateral facet are opposite, the

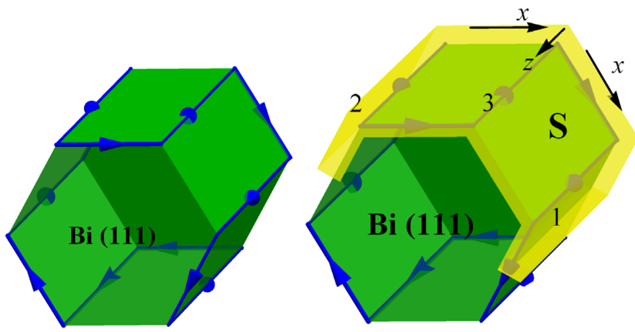

FIG. 1. Left: In a Bi(111) nanowire (green), the gapless states (blue arrows) propagate along the hinges. The spin-up (-down) hinge states move against (along) the directions of the arrows. The helicities of any two parallel hinge states [along $z \equiv (111)$ axis] on a single lateral facet are opposite. Right: In the proposed setup, a superconducting layer (yellow) covers three parallel hinges (labeled by 1, 2, and 3). The (1,2) pair carries the same helicity, allowing for the crossed Andreev pairing. For other pairs, [(1,3) and (2,3)], such pairing is suppressed. The x axis of the local coordinate is defined along the perimeter of the hexagonal cross section, and the y axis (not shown) is normal to the lateral facets.

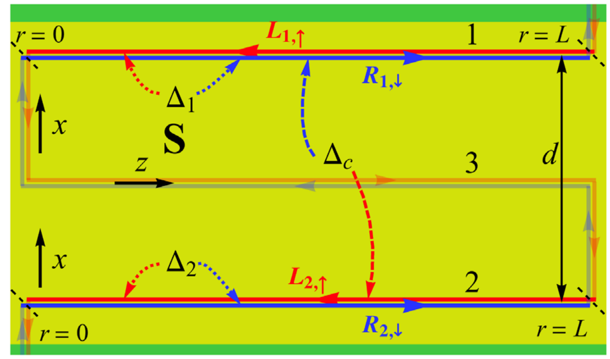

FIG. 2. Schematics of the parahelical setup in the xz plane of the local coordinate (view from the $+y$ direction) with the hinge coordinate r. A superconductor (yellow) covers three long hinges (along the z direction), and several short hinges (along the x direction). In hinges 1 and 2, which are at distance d, the spin-up states propagate toward the $-r$ direction (red solid arrows) while the spin-down states toward $+r$ (blue solid arrows). Hinge 3 is decoupled from the others. The local ($\Delta_{1,2}$) and crossed Andreev (Δ_c) pairing processes are indicated by the dotted and dashed arrows, respectively. Since the short segments along the x direction are not aligned in the laboratory frame, Δ_c is suppressed if $r \notin [0, L]$, while $\Delta_{1,2}$ remains constant for any r, including in the short segments. As a result, the boundaries (black dashed lines) are created at $r = 0$ and $r = L$ (the ends of the nanowire), which are assumed to be far apart on the scale of the Majorana localization length. For clarity, only one crossed Andreev pairing process, $\Delta_c R^\dagger_{1,\downarrow} L^\dagger_{2,\uparrow}$, is depicted.

orthohelical setup is realized when a superconductor covers one lateral facet with two parallel hinges. In this case, crossed Andreev pairing is not feasible.

However, when the superconductor extends over two lateral facets (see the right panel of Fig. 1), it is in contact with three parallel hinges along $z \equiv (111)$ axis. Two of them (labeled by 1 and 2) carry the same helicity while the third one (labeled by 3) the opposite. The momentum selection rules, together with uniform chemical potential (assumed to be in the bulk gap and not very close to the Dirac point) allow a crossed Andreev pairing between the hinges 1 and 2 and forbid it between the orthohelical hinges [(1,3) and (2,3) pairs], see Fig. 2. As a result, the hinge 3 decouples from the remaining two and the parahelical setup is realized in the hinges 1 and 2 [97].

Model.—From now on we restrict our work to the two coupled hinges [100]. We model them using the fields

$$\psi_n(r) = R_{n,\downarrow}(r) e^{ik_F r} + L_{n,\uparrow}(r) e^{-ik_F r}, \quad (1)$$

with the coordinate r along the hinge, the hinge index $n \in \{1, 2\}$, the Fermi wave number k_F, and the slowly varying right- and left-moving fields $R_{n,\downarrow}$ and $L_{n,\uparrow}$, respectively. Whenever possible, we suppress the coordinate r and the spin index, the latter fixed by the spin-momentum locking. In a noninteracting system, the effective Hamiltonian reads $H = H_0 + H_{\text{intra}} + H_c$. The kinetic energy term is

$$H_0 = -i\hbar v_F \sum_{n=1,2} \int dr (R^\dagger_n \partial_r R_n - L^\dagger_n \partial_r L_n), \quad (2)$$

with the Fermi velocity v_F. The local pairing term is

$$H_{\text{intra}} = \sum_{n=1,2} \int dr \left[\frac{\Delta_n}{2} (R^\dagger_n L^\dagger_n - L^\dagger_n R^\dagger_n) + \text{H.c.} \right], \quad (3)$$

with the pairing gap Δ_n in the hinge n. Finally, the crossed Andreev pairing term is

$$H_c = \int dr \left[\frac{\Delta_c}{2} (R^\dagger_1 L^\dagger_2 - L^\dagger_2 R^\dagger_1) + (1 \leftrightarrow 2) \right] + \text{H.c.}, \quad (4)$$

with the pairing gap Δ_c. For simplicity, we take a spatially uniform real local pairing gap $\Delta_n > 0$. On the other hand, the crossed Andreev pairing gap Δ_c changes its (real) value from finite ($r \in [0, L]$) to zero ($r \notin [0, L]$), creating two boundaries at $r = 0$ and $r = L$, as indicated in Fig. 2. Assuming the hinge length L being sufficiently long, we focus only on the boundary at $r = 0$ and demonstrate the existence of a MKP localized there.

Majorana Kramers pairs.—We first identify the criterion for MKPs in a noninteracting system. The single-particle Hamiltonian, see Eqs. (2)–(4), can be written in the basis $\Psi = (R_1, L_1, R_2, L_2, R^\dagger_1, L^\dagger_1, R^\dagger_2, L^\dagger_2)^T$ as $H = \frac{1}{2} \int dr \Psi^\dagger(r) \mathcal{H}(r) \Psi(r)$, with the Hamiltonian density

$$\mathcal{H}(r) = -i\hbar v_F \eta^0 \tau^0 \sigma^z \partial_r - \Delta_+ \eta^y \tau^0 \sigma^y - \Delta_- \eta^y \tau^z \sigma^y - \Delta_c \eta^y \tau^x \sigma^y, \quad (5)$$

with $\Delta_\pm = (\Delta_1 \pm \Delta_2)/2$. In the above, the matrices η^μ, τ^μ, and σ^μ act on the particle hole, hinge, and spin space, respectively. They are given by the Pauli (identity) matrix for $\mu = x, y, z$ ($\mu = 0$). The bulk spectrum is twofold degenerate due to the time-reversal symmetry (TRS), with a gap denoted as Δ_b. The reversal of the sign of Δ_b, which can be shown to coincide with the sign of $(\Delta_1\Delta_2 - \Delta_c^2)$, indicates the band inversion and suggests the presence of zero-energy MBSs at a boundary.

By directly solving the Bogoliubov–de Gennes equation of Eq. (5) at zero energy [65,101], one can show that such bound states are indeed present [97]. With this procedure, we find that a MKP at $r = 0$ (and another pair at $r = L$) emerges if and only if

$$\Delta_c^2 > \Delta_1 \Delta_2. \quad (6)$$

Because of its topological origin, the MKP appears and disappears wherever Δ_b reverses its sign even in setups with different model details, e.g., a less abrupt change of Δ_c. Similarly, additional second-order (co-)tunneling processes [68,72,102] not included here do not affect the topological criterion as long as the local pairing gaps Δ_n are of similar strengths [97]. We therefore conclude that the criterion for MKPs is the crossed Andreev pairing to be dominant over the local pairing, as described by Eq. (6). In noninteracting systems, however, Eq. (6) cannot be fulfilled [102]. Including electron-electron interactions is thus essential for our scheme. Below we demonstrate that even moderate interactions can drive the system into the topological superconducting phase hosting MKPs.

Interacting system.—To begin, we note that since our setup respects TRS, the elastic backscattering is precluded in the helical channels (unless the TRS is broken, for example, by nuclear spins [103,104]). We therefore include only the forward scattering processes into the interaction $H_{\rm int}$ and bosonize the total hinge Hamiltonian $H_{\rm el} = H_0 + H_{\rm int}$. This procedure leads to two copies of the helical Tomonaga-Luttinger liquid,

$$H_{\rm el} = \sum_{n=1,2} \int \frac{\hbar dr}{2\pi} \left\{ u_n K_n [\partial_r \theta_n(r)]^2 + \frac{u_n}{K_n} [\partial_r \phi_n(r)]^2 \right\}, \quad (7)$$

with the interaction parameter K_n for the hinge n and the modified velocity $u_n = v_F/K_n$. Using standard bosonic fields θ_n and ϕ_n for helical channels [103,104], the local pairing term reads

$$H_{\rm intra} = \sum_{n=1,2} \frac{\Delta_n}{\pi a} \int dr \cos[2\theta_n(r)], \quad (8)$$

where a is the short-distance cutoff, taken to be the transverse decay length of the hinge states. The crossed Andreev pairing term is

$$H_c = \frac{2\Delta_c}{\pi a} \int dr \cos[\theta_1(r) + \theta_2(r)] \cos[\phi_1(r) - \phi_2(r)]. \quad (9)$$

Above certain interaction strength, the crossed Andreev pairing dominates and the topological criterion [see Eq. (6)] is satisfied. To show this, we derive the renormalization-group (RG) flow equations [97] following standard procedure [105]. To simplify the analysis, we introduce the dimensionless coupling constants,

$$\tilde{\Delta}_n(l) = \frac{\Delta_n(l)a(l)}{\hbar u_n}, \qquad \tilde{\Delta}_c(l) = \frac{\Delta_c(l)a(l)}{\hbar\sqrt{u_1 u_2}}, \quad (10)$$

with $l \equiv \ln[a(l)/a(0)]$. For given initial parameters (at $l = 0$), we numerically propagate the RG flow equations. We stop the RG flow whenever any of the dimensionless coupling constants becomes unity. At these points we obtain the renormalized gaps and evaluate the criterion for the MKP existence.

An example of the RG flow is in Fig. 3, showing how the pairing gaps evolve for several starting values. The repulsive interaction tends to reduce both types of the pairing. Importantly, due to the local nature of the Coulomb interaction, the suppression is stronger for the local pairing (red dashed curve) than for the crossed Andreev pairing (blue solid curve): the repulsive interaction favors the nonlocal pairing. Consequently, even if in their initial values the local pairing dominates over the crossed Andreev pairing [we take $\tilde{\Delta}_c(0)/\tilde{\Delta}_1(0) = 1/3$ in Fig. 3], a sufficiently strong interaction can reverse this relation.

To prove that Eq. (6) with the renormalized pairing gaps is the correct criterion, we note that the end points of the RG flows (green arrows) are adiabatically connected to the noninteracting limit without closing the bulk gap. Here, the model can be refermionized into Eq. (5) with renormalized pairing gaps [106]. The refermionized model can be used to justify the existence of MKPs and allows us to estimate their localization length. It is typically around 20 nm and much shorter than the hinge length $L \sim 1$ μm [97]. We thus conclude that sufficiently strong electron-electron interactions can stabilize well isolated MKPs.

Phase diagram.—To investigate the stability of the MKPs in the parameter space, we repeat the above numerical procedure for $K_1(0) \in [0, 1]$ and $\Delta_1(0)/\Delta_c(0) \in [1, 7]$, see Fig. 4. In the phase diagram, the green (yellow) color stands for the region in which MKPs are present (absent). If the system is noninteracting, the MKPs are absent, consistent

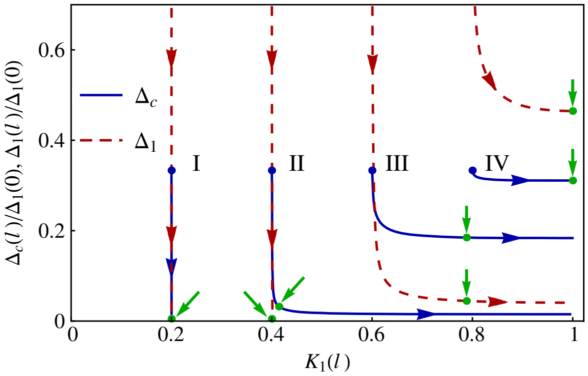

FIG. 3. RG flow diagram. We take the parameters $K_1(0) = K_2(0) = 0.2, 0.4, 0.6$, and 0.8, $\tilde{\Delta}_1(0) = \tilde{\Delta}_2(0) = 3\tilde{\Delta}_c(0) = 0.03$, $a(0) = 5$ nm, and $L = 1$ μm. The crossed Andreev (local) pairing gap Δ_c ($\Delta_1 = \Delta_2$) is plotted in blue solid (red dashed) curves. The blue dots (labeled by I–IV) mark the initial points of Δ_c, and the green arrows and points specify where the RG flows stop. The RG flows labeled by II and III stop at the points at which the renormalized crossed Andreev pairing dominates over the local pairing ($\Delta_c > \Delta_1$), indicating the topological superconducting phase.

with Ref. [102]. For $\Delta_1(0)/\Delta_c(0) \gtrsim 1$, a rather weak interaction $K_n(0) \lesssim 1$ can stabilize the MKPs. The larger $\Delta_1(0)/\Delta_c(0)$ is, the stronger interaction is required to reverse the gap strengths. A very strong interaction [red region; $K_1(0) < 2 - \sqrt{3} \approx 0.27$] destroys both types of the pairing

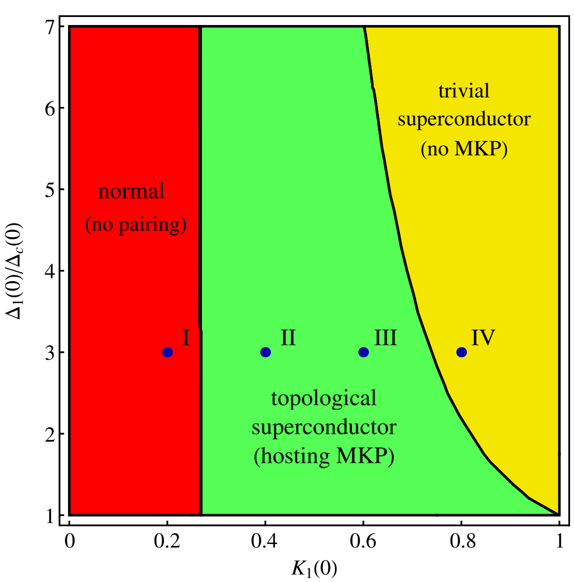

FIG. 4. Phase diagram. The vertical and horizontal axes label the initial values of the gap ratio $[\Delta_1(0)/\Delta_c(0)]$ and interaction parameter $K_1(0) = K_2(0)$, respectively. The other parameters are the same as those in Fig. 3. The green (yellow) region marks the phase with (without) MKPs. The corresponding RG flows to the blue dots (labeled by I–IV) are shown in Fig. 3. In the red region, both types of the pairing gaps vanish.

gaps. Further, we estimate the initial values $K_1(0) \lesssim 0.6$ [107] and $\Delta_1(0)/\Delta_c(0) = O(1)$ [97], and find that they are compatible with the MKP regime in Fig. 4.

In comparison with nonhelical nanowires [73], our setup requires weaker interactions to induce MKPs. The difference between nonhelical and helical channels can be understood as follows. The effects of electron-electron interactions in nonhelical channels are "averaged" over charge and (noninteracting) spin sectors, and thus weakened as compared to helical channels. This quantitative difference indicates the advantage of helical channels, making HOTIs a promising platform for topological superconductivity without the need of magnetic fields.

The same RG analysis performed in the standard but more involved source-term approach [73,108], in which one incorporates explicitly the interhinge separation d and coherence length ξ_s of the superconductor instead of relying on knowing initial values of $\Delta_1(0)$ and $\Delta_c(0)$ in the effective Hamiltonian, gives essentially the same phase diagram as in Fig. 4; see Ref. [97]. For the parameters of bismuth hinges [80,93,109], we find that moderate interactions can render a dominant crossed Andreev pairing for $d \sim 100$ nm and $\xi_s \sim 1$ μm. With these quantitative examinations [97], we conclude that our setup is accessible in realistic samples.

Discussion.—Our work indicates that generally MKPs can be supported at the ends of a HOTI nanowire proximity coupled to a superconductor without fine-tuning. We remark that the hinge states are known to survive even when spatial symmetries are broken by weak local perturbations due to disorder, as long as the TRS is preserved [80]. As a consequence, the MKPs proposed in this work are robust against TRS-preserving disorder. It is also worth pointing out that, in addition to the MKPs, our setup can work as a Cooper pair splitter—a source of spatially separated spin-entangled electron pairs [110–122]. Finally, we remark that detection of MKPs with the parity-controlled 2π Josephson effect, which gives distinct signatures from unpaired MBSs [123], and braiding-based [124,125] or measurement-based [126] quantum computation schemes utilizing MKPs have been widely discussed in the literature. Compared to setups without TRS, since here the MKPs require no magnetic fields, they are protected by a larger superconducting gap, leading to shorter localization length and longer coherence time [72,126]. Our setup provides building blocks for the measurement-based structures proposed in Refs. [127–129], which offers a route to scalable architectures for topological quantum computation.

We thank R. S. Deacon for helpful discussion. This work was supported financially by the JSPS Kakenhi Grant No. 16H02204, by the Swiss National Science Foundation (Switzerland), and by the NCCR QSIT. This project received funding from the European Unions Horizon 2020 research and innovation program (ERC Starting Grant, Grant Agreement No. 757725).

[1] A. Y. Kitaev, Unpaired Majorana fermions in quantum wires, Phys. Usp. **44**, 131 (2001).

[2] A. Y. Kitaev, Fault-tolerant quantum computation by anyons, Ann. Phys. (Amsterdam) **303**, 2 (2003).

[3] C. Nayak, S. H. Simon, A. Stern, M. Freedman, and S. Das Sarma, Non-Abelian anyons and topological quantum computation, Rev. Mod. Phys. **80**, 1083 (2008).

[4] Y. Tanaka, T. Yokoyama, and N. Nagaosa, Manipulation of the Majorana Fermion, Andreev Reflection, and Josephson Current on Topological Insulators, Phys. Rev. Lett. **103**, 107002 (2009).

[5] M. Sato and S. Fujimoto, Topological phases of non-centrosymmetric superconductors: Edge states, Majorana fermions, and non-Abelian statistics, Phys. Rev. B **79**, 094504 (2009).

[6] M. Z. Hasan and C. L. Kane, Colloquium: Topological insulators, Rev. Mod. Phys. **82**, 3045 (2010).

[7] X.-L. Qi and S.-C. Zhang, Topological insulators and superconductors, Rev. Mod. Phys. **83**, 1057 (2011).

[8] J. Alicea, Y. Oreg, G. Refael, F. von Oppen, and M. P. A. Fisher, Non-Abelian statistics and topological quantum information processing in 1D wire networks, Nat. Phys. **7**, 412 (2011).

[9] A. Cook and M. Franz, Majorana fermions in a topological-insulator nanowire proximity-coupled to an s-wave superconductor, Phys. Rev. B **84**, 201105 (2011).

[10] J. Klinovaja, P. Stano, and D. Loss, Transition from Fractional to Majorana Fermions in Rashba Nanowires, Phys. Rev. Lett. **109**, 236801 (2012).

[11] D. Chevallier, D. Sticlet, P. Simon, and C. Bena, Mutation of Andreev into Majorana bound states in long superconductor-normal and superconductor-normal-superconductor junctions, Phys. Rev. B **85**, 235307 (2012).

[12] F. Domínguez, F. Hassler, and G. Platero, Dynamical detection of Majorana fermions in current-biased nanowires, Phys. Rev. B **86**, 140503 (2012).

[13] J. Klinovaja, S. Gangadharaiah, and D. Loss, Electric-Field-Induced Majorana Fermions in Armchair Carbon Nanotubes, Phys. Rev. Lett. **108**, 196804 (2012).

[14] Y. Niu, S. B. Chung, C.-H. Hsu, I. Mandal, S. Raghu, and S. Chakravarty, Majorana zero modes in a quantum Ising chain with longer-ranged interactions, Phys. Rev. B **85**, 035110 (2012).

[15] E. Prada, P. San-Jose, and R. Aguado, Transport spectroscopy of NS nanowire junctions with Majorana fermions, Phys. Rev. B **86**, 180503 (2012).

[16] B. M. Terhal, F. Hassler, and D. P. DiVincenzo, From Majorana Fermions to Topological Order, Phys. Rev. Lett. **108**, 260504 (2012).

[17] C. Beenakker, Search for Majorana fermions in superconductors, Annu. Rev. Condens. Matter Phys. **4**, 113 (2013).

[18] K. Björnson and A. M. Black-Schaffer, Vortex states and Majorana fermions in spin-orbit coupled semiconductor-superconductor hybrid structures, Phys. Rev. B **88**, 024501 (2013).

[19] S. Nakosai, J. C. Budich, Y. Tanaka, B. Trauzettel, and N. Nagaosa, Majorana Bound States and Nonlocal Spin Correlations in a Quantum Wire on an Unconventional Superconductor, Phys. Rev. Lett. **110**, 117002 (2013).

[20] M. Thakurathi, A. A. Patel, D. Sen, and A. Dutta, Floquet generation of Majorana end modes and topological invariants, Phys. Rev. B **88**, 155133 (2013).

[21] E. Dumitrescu, J. D. Sau, and S. Tewari, Magnetic field response and chiral symmetry of time-reversal-invariant topological superconductors, Phys. Rev. B **90**, 245438 (2014).

[22] F. Maier, J. Klinovaja, and D. Loss, Majorana fermions in Ge/Si hole nanowires, Phys. Rev. B **90**, 195421 (2014).

[23] L. Weithofer, P. Recher, and T. L. Schmidt, Electron transport in multiterminal networks of Majorana bound states, Phys. Rev. B **90**, 205416 (2014).

[24] R. S. Deacon, J. Wiedenmann, E. Bocquillon, F. Domínguez, T. M. Klapwijk, P. Leubner, C. Brüne, E. M. Hankiewicz, S. Tarucha, K. Ishibashi, H. Buhmann, and L. W. Molenkamp, Josephson Radiation from Gapless Andreev Bound States in HgTe-Based Topological Junctions, Phys. Rev. X **7**, 021011 (2017).

[25] G.-Y. Huang and H. Q. Xu, Majorana fermions in topological-insulator nanowires: From single superconducting nanowires to Josephson junctions, Phys. Rev. B **95**, 155420 (2017).

[26] W. Izumida, L. Milz, M. Marganska, and M. Grifoni, Topology and zero energy edge states in carbon nanotubes with superconducting pairing, Phys. Rev. B **96**, 125414 (2017).

[27] J. Manousakis, A. Altland, D. Bagrets, R. Egger, and Y. Ando, Majorana qubits in a topological insulator nanoribbon architecture, Phys. Rev. B **95**, 165424 (2017).

[28] A. Ptok, A. Kobiałka, and T. Domański, Controlling the bound states in a quantum-dot hybrid nanowire, Phys. Rev. B **96**, 195430 (2017).

[29] M. Sato and Y. Ando, Topological superconductors: A review, Rep. Prog. Phys. **80**, 076501 (2017).

[30] C. Reeg, D. Loss, and J. Klinovaja, Proximity effect in a two-dimensional electron gas coupled to a thin superconducting layer, Beilstein J. Nanotechnol. **9**, 1263 (2018).

[31] M. Trif, O. Dmytruk, H. Bouchiat, R. Aguado, and P. Simon, Dynamic current susceptibility as a probe of Majorana bound states in nanowire-based Josephson junctions, Phys. Rev. B **97**, 041415 (2018).

[32] R. M. Lutchyn, J. D. Sau, and S. Das Sarma, Majorana Fermions and a Topological Phase Transition in Semiconductor-Superconductor Heterostructures, Phys. Rev. Lett. **105**, 077001 (2010).

[33] Y. Oreg, G. Refael, and F. von Oppen, Helical Liquids and Majorana Bound States in Quantum Wires, Phys. Rev. Lett. **105**, 177002 (2010).

[34] V. Mourik, K. Zuo, S. M. Frolov, S. R. Plissard, E. P. A. M. Bakkers, and L. P. Kouwenhoven, Signatures of Majorana fermions in hybrid superconductor-semiconductor nanowire devices, Science **336**, 1003 (2012).

[35] A. Das, Y. Ronen, Y. Most, Y. Oreg, M. Heiblum, and H. Shtrikman, Zero-bias peaks and splitting in an InAs nanowire topological superconductor as a signature of Majorana fermions, Nat. Phys. **8**, 887 (2012).

[36] M. T. Deng, C. L. Yu, G. Y. Huang, M. Larsson, P. Caroff, and H. Q. Xu, Anomalous zero-bias conductance peak in a Nb–InSb nanowire–Nb hybrid device, Nano Lett. **12**, 6414 (2012).

[37] L. P. Rokhinson, X. Liu, and J. K. Furdyna, The fractional a.c. Josephson effect in a semiconductor–superconductor nanowire as a signature of Majorana particles, Nat. Phys. **8**, 795 (2012).
[38] A. D. K. Finck, D. J. Van Harlingen, P. K. Mohseni, K. Jung, and X. Li, Anomalous Modulation of a Zero-Bias Peak in a Hybrid Nanowire-Superconductor Device, Phys. Rev. Lett. **110**, 126406 (2013).
[39] H. O. H. Churchill, V. Fatemi, K. Grove-Rasmussen, M. T. Deng, P. Caroff, H. Q. Xu, and C. M. Marcus, Superconductor-nanowire devices from tunneling to the multichannel regime: Zero-bias oscillations and magnetoconductance crossover, Phys. Rev. B **87**, 241401 (2013).
[40] D. Rainis, L. Trifunovic, J. Klinovaja, and D. Loss, Towards a realistic transport modeling in a superconducting nanowire with Majorana fermions, Phys. Rev. B **87**, 024515 (2013).
[41] S. Takei, B. M. Fregoso, H.-Y. Hui, A. M. Lobos, and S. Das Sarma, Soft Superconducting Gap in Semiconductor Majorana Nanowires, Phys. Rev. Lett. **110**, 186803 (2013).
[42] S. M. Albrecht, A. P. Higginbotham, M. Madsen, F. Kuemmeth, T. S. Jespersen, J. Nygård, P. Krogstrup, and C. M. Marcus, Exponential protection of zero modes in Majorana islands, Nature (London) **531**, 206 (2016).
[43] O. Gül, H. Zhang, J. D. S. Bommer, M. W. A. de Moor, D. Car, S. R. Plissard, E. P. A. M. Bakkers, A. Geresdi, K. Watanabe, T. Taniguchi, and L. P. Kouwenhoven, Ballistic Majorana nanowire devices, Nat. Nanotechnol. **13**, 192 (2018).
[44] H. Zhang *et al.*, Quantized Majorana conductance, Nature (London) **556**, 74 (2018).
[45] L. Fu and C. L. Kane, Superconducting Proximity Effect and Majorana Fermions at the Surface of a Topological Insulator, Phys. Rev. Lett. **100**, 096407 (2008).
[46] L. Fu and C. L. Kane, Josephson current and noise at a superconductor/quantum-spin-Hall-insulator/superconductor junction, Phys. Rev. B **79**, 161408 (2009).
[47] R. Skolasinski, D. I. Pikulin, J. Alicea, and M. Wimmer, Robust helical edge transport in quantum spin hall quantum wells, arXiv:1709.04830.
[48] H. Zhang, C.-X. Liu, X.-L. Qi, X. Dai, Z. Fang, and S.-C. Zhang, Topological insulators in Bi_2Se_3, Bi_2Te_3 and Sb_2Te_3 with a single Dirac cone on the surface, Nat. Phys. **5**, 438 (2009).
[49] D. Hsieh, Y. Xia, D. Qian, L. Wray, F. Meier, J. H. Dil, J. Osterwalder, L. Patthey, A. V. Fedorov, H. Lin, A. Bansil, D. Grauer, Y. S. Hor, R. J. Cava, and M. Z. Hasan, Observation of Time-Reversal-Protected Single-Dirac-Cone Topological-Insulator States in Bi_2Te_3 and Sb_2Te_3, Phys. Rev. Lett. **103**, 146401 (2009).
[50] C. Brüne, C. X. Liu, E. G. Novik, E. M. Hankiewicz, H. Buhmann, Y. L. Chen, X. L. Qi, Z. X. Shen, S. C. Zhang, and L. W. Molenkamp, Quantum Hall Effect from the Topological Surface States of Strained Bulk HgTe, Phys. Rev. Lett. **106**, 126803 (2011).
[51] C.-A. Li, S.-B. Zhang, and S.-Q. Shen, Hidden edge Dirac point and robust quantum edge transport in InAs/GaSb quantum wells, Phys. Rev. B **97**, 045420 (2018).
[52] A. Keselman, L. Fu, A. Stern, and E. Berg, Inducing Time-Reversal-Invariant Topological Superconductivity and Fermion Parity Pumping in Quantum Wires, Phys. Rev. Lett. **111**, 116402 (2013).
[53] A. Haim, A. Keselman, E. Berg, and Y. Oreg, Time-reversal-invariant topological superconductivity induced by repulsive interactions in quantum wires, Phys. Rev. B **89**, 220504 (2014).
[54] C. Schrade, A. A. Zyuzin, J. Klinovaja, and D. Loss, Proximity-induced π Josephson Junctions in Topological Insulators and Kramers Pairs of Majorana Fermions, Phys. Rev. Lett. **115**, 237001 (2015).
[55] C. L. M. Wong and K. T. Law, Majorana Kramers doublets in $d_{x^2-y^2}$-wave superconductors with Rashba spin-orbit coupling, Phys. Rev. B **86**, 184516 (2012).
[56] F. Zhang, C. L. Kane, and E. J. Mele, Time-Reversal-Invariant Topological Superconductivity and Majorana Kramers Pairs, Phys. Rev. Lett. **111**, 056402 (2013).
[57] S. Hoffman, J. Klinovaja, and D. Loss, Topological phases of inhomogeneous superconductivity, Phys. Rev. B **93**, 165418 (2016).
[58] Z. Yan, F. Song, and Z. Wang, Majorana Corner Modes in a High-Temperature Platform, Phys. Rev. Lett. **121**, 096803 (2018).
[59] J. Klinovaja, P. Stano, A. Yazdani, and D. Loss, Topological Superconductivity and Majorana Fermions in RKKY Systems, Phys. Rev. Lett. **111**, 186805 (2013).
[60] B. Braunecker and P. Simon, Interplay between Classical Magnetic Moments and Superconductivity in Quantum One-Dimensional Conductors: Toward a Self-Sustained Topological Majorana Phase, Phys. Rev. Lett. **111**, 147202 (2013).
[61] M. M. Vazifeh and M. Franz, Self-Organized Topological State with Majorana Fermions, Phys. Rev. Lett. **111**, 206802 (2013).
[62] S. Nadj-Perge, I. K. Drozdov, B. A. Bernevig, and A. Yazdani, Proposal for realizing Majorana fermions in chains of magnetic atoms on a superconductor, Phys. Rev. B **88**, 020407 (2013).
[63] S. Nadj-Perge, I. K. Drozdov, J. Li, H. Chen, S. Jeon, J. Seo, A. H. MacDonald, B. A. Bernevig, and A. Yazdani, Observation of Majorana fermions in ferromagnetic atomic chains on a superconductor, Science **346**, 602 (2014).
[64] F. Pientka, L. I. Glazman, and F. von Oppen, Unconventional topological phase transitions in helical Shiba chains, Phys. Rev. B **89**, 180505 (2014).
[65] C.-H. Hsu, P. Stano, J. Klinovaja, and D. Loss, Antiferromagnetic nuclear spin helix and topological superconductivity in ^{13}C nanotubes, Phys. Rev. B **92**, 235435 (2015).
[66] R. Pawlak, M. Kisiel, J. Klinovaja, T. Meier, S. Kawai, T. Glatzel, D. Loss, and E. Meyer, Probing atomic structure and Majorana wavefunctions in mono-atomic Fe chains on superconducting Pb surface, npj Quantum Inf. **2**, 16035 (2016).
[67] E. Gaidamauskas, J. Paaske, and K. Flensberg, Majorana Bound States in Two-Channel Time-Reversal-Symmetric Nanowire Systems, Phys. Rev. Lett. **112**, 126402 (2014).
[68] J. Klinovaja, A. Yacoby, and D. Loss, Kramers pairs of Majorana fermions and parafermions in fractional topological insulators, Phys. Rev. B **90**, 155447 (2014).

[69] J. Klinovaja and D. Loss, Time-reversal invariant parafermions in interacting Rashba nanowires, Phys. Rev. B **90**, 045118 (2014).

[70] J. Klinovaja and D. Loss, Fractional charge and spin states in topological insulator constrictions, Phys. Rev. B **92**, 121410 (2015).

[71] H. Ebisu, B. Lu, J. Klinovaja, and Y. Tanaka, Theory of time-reversal topological superconductivity in double Rashba wires: Symmetries of Cooper pairs and Andreev bound states, Prog. Theor. Exp. Phys. **2016**, 083I01 (2016).

[72] C. Schrade, M. Thakurathi, C. Reeg, S. Hoffman, J. Klinovaja, and D. Loss, Low-field topological threshold in Majorana double nanowires, Phys. Rev. B **96**, 035306 (2017).

[73] M. Thakurathi, P. Simon, I. Mandal, J. Klinovaja, and D. Loss, Majorana Kramers pairs in Rashba double nanowires with interactions and disorder, Phys. Rev. B **97**, 045415 (2018).

[74] W. A. Benalcazar, B. A. Bernevig, and T. L. Hughes, Quantized electric multipole insulators, Science **357**, 61 (2017).

[75] W. A. Benalcazar, B. A. Bernevig, and T. L. Hughes, Electric multipole moments, topological multipole moment pumping, and chiral hinge states in crystalline insulators, Phys. Rev. B **96**, 245115 (2017).

[76] F. Schindler, A. M. Cook, M. G. Vergniory, Z. Wang, S. S. P. Parkin, B. A. Bernevig, and T. Neupert, Higher-order topological insulators, Sci. Adv. **4**, eaat0346 (2018).

[77] J. Langbehn, Y. Peng, L. Trifunovic, F. von Oppen, and P. W. Brouwer, Reflection-Symmetric Second-Order Topological Insulators and Superconductors, Phys. Rev. Lett. **119**, 246401 (2017).

[78] Z. Song, Z. Fang, and C. Fang, $(d-2)$-Dimensional Edge States of Rotation Symmetry Protected Topological States, Phys. Rev. Lett. **119**, 246402 (2017).

[79] M. Ezawa, Higher-Order Topological Insulators and Semimetals on the Breathing Kagome and Pyrochlore Lattices, Phys. Rev. Lett. **120**, 026801 (2018).

[80] F. Schindler, Z. Wang, M. G. Vergniory, A. M. Cook, A. Murani, S. Sengupta, A. Y. Kasumov, R. Deblock, S. Jeon, I. Drozdov, H. Bouchiat, S. Guéron, A. Yazdani, B. A. Bernevig, and T. Neupert, Higher-order topology in bismuth, Nat. Phys. **14**, 918 (2018).

[81] E. Khalaf, Higher-order topological insulators and superconductors protected by inversion symmetry, Phys. Rev. B **97**, 205136 (2018).

[82] C. Beenakker, Mystery solved of the sawtooth Josephson effect in bismuth, https://www.condmatjclub.org/?p=3319.

[83] L. Fu, C. L. Kane, and E. J. Mele, Topological Insulators in Three Dimensions, Phys. Rev. Lett. **98**, 106803 (2007).

[84] J. E. Moore and L. Balents, Topological invariants of time-reversal-invariant band structures, Phys. Rev. B **75**, 121306 (2007).

[85] D. Hsieh, D. Qian, L. Wray, Y. Xia, Y. S. Hor, R. J. Cava, and M. Z. Hasan, A topological Dirac insulator in a quantum spin Hall phase, Nature (London) **452**, 970 (2008).

[86] R. Roy, Topological phases and the quantum spin Hall effect in three dimensions, Phys. Rev. B **79**, 195322 (2009).

[87] C. L. Kane and E. J. Mele, Z_2 Topological Order and the Quantum Spin Hall Effect, Phys. Rev. Lett. **95**, 146802 (2005).

[88] C. L. Kane and E. J. Mele, Quantum Spin Hall Effect in Graphene, Phys. Rev. Lett. **95**, 226801 (2005).

[89] B. A. Bernevig and S.-C. Zhang, Quantum Spin Hall Effect, Phys. Rev. Lett. **96**, 106802 (2006).

[90] B. A. Bernevig, T. L. Hughes, and S.-C. Zhang, Quantum spin hall effect and topological phase transition in HgTe quantum wells, Science **314**, 1757 (2006).

[91] S. Murakami, Quantum Spin Hall Effect and Enhanced Magnetic Response by Spin-Orbit Coupling, Phys. Rev. Lett. **97**, 236805 (2006).

[92] C. Liu, T. L. Hughes, X.-L. Qi, K. Wang, and S.-C. Zhang, Quantum Spin Hall Effect in Inverted Type-II Semiconductors, Phys. Rev. Lett. **100**, 236601 (2008).

[93] M. Wada, S. Murakami, F. Freimuth, and G. Bihlmayer, Localized edge states in two-dimensional topological insulators: Ultrathin Bi films, Phys. Rev. B **83**, 121310 (2011).

[94] I. K. Drozdov, A. Alexandradinata, S. Jeon, S. Nadj-Perge, H. Ji, R. J. Cava, B. A. Bernevig, and A. Yazdani, One-dimensional topological edge states of bismuth bilayers, Nat. Phys. **10**, 664 (2014).

[95] A. Murani, A. Kasumov, S. Sengupta, Y. A. Kasumov, V. T. Volkov, I. I. Khodos, F. Brisset, R. Delagrange, A. Chepelianskii, R. Deblock, H. Bouchiat, and S. Guéron, Ballistic edge states in bismuth nanowires revealed by SQUID interferometry, Nat. Commun. **8**, 15941 (2017).

[96] Even though bismuth is a bulk semimetal, the topologically trivial bulk states can be gapped by, e.g., superconductivity, disorder or finite-size effects [80,82,91,93,95]. Further, while we take Bi(111) nanowires as an example, our setup can be implemented also in other recently predicted helical HOTI materials, such as SnTe, Bi_2TeI, BiSe, and BiTe [76].

[97] See Supplemental Material at http://link.aps.org/supplemental/10.1103/PhysRevLett.121.196801 for the technical details, which includes Refs. [98,99].

[98] T. L. Schmidt, S. Rachel, F. von Oppen, and L. I. Glazman, Inelastic Electron Backscattering in a Generic Helical Edge Channel, Phys. Rev. Lett. **108**, 156402 (2012).

[99] M. G. Vergniory, L. Elcoro, C. Felser, B. A. Bernevig, and Z. Wang, The (high quality) topological materials in the world, arXiv:1807.10271.

[100] We consider a clean system with identical Fermi wave numbers for the two identical hinges. However, our results are robust against weak disorder [97].

[101] J. Klinovaja and D. Loss, Composite Majorana fermion wave functions in nanowires, Phys. Rev. B **86**, 085408 (2012).

[102] C. Reeg, J. Klinovaja, and D. Loss, Destructive interference of direct and crossed Andreev pairing in a system of two nanowires coupled via an *s*-wave superconductor, Phys. Rev. B **96**, 081301 (2017).

[103] C.-H. Hsu, P. Stano, J. Klinovaja, and D. Loss, Nuclear-spin-induced localization of edge states in two-dimensional topological insulators, Phys. Rev. B **96**, 081405 (2017).
[104] C.-H. Hsu, P. Stano, J. Klinovaja, and D. Loss, Effects of nuclear spins on the transport properties of the edge of two-dimensional topological insulators, Phys. Rev. B **97**, 125432 (2018).
[105] T. Giamarchi, *Quantum Physics in One Dimension* (Oxford University Press, New York, 2003).
[106] S. Gangadharaiah, B. Braunecker, P. Simon, and D. Loss, Majorana Edge States in Interacting One-Dimensional Systems, Phys. Rev. Lett. **107**, 036801 (2011).
[107] J. Maciejko, C. Liu, Y. Oreg, X.-L. Qi, C. Wu, and S.-C. Zhang, Kondo Effect in the Helical Edge Liquid of the Quantum Spin Hall State, Phys. Rev. Lett. **102**, 256803 (2009).
[108] P. Virtanen and P. Recher, Signatures of Rashba spin-orbit interaction in the superconducting proximity effect in helical Luttinger liquids, Phys. Rev. B **85**, 035310 (2012).
[109] Y. M. Koroteev, G. Bihlmayer, E. V. Chulkov, and S. Blügel, First-principles investigation of structural and electronic properties of ultrathin Bi films, Phys. Rev. B **77**, 045428 (2008).
[110] P. Recher, E. V. Sukhorukov, and D. Loss, Andreev tunneling, Coulomb blockade, and resonant transport of nonlocal spin-entangled electrons, Phys. Rev. B **63**, 165314 (2001).
[111] P. Recher and D. Loss, Superconductor coupled to two Luttinger liquids as an entangler for electron spins, Phys. Rev. B **65**, 165327 (2002).
[112] C. Bena, S. Vishveshwara, L. Balents, and M. P. A. Fisher, Quantum Entanglement in Carbon Nanotubes, Phys. Rev. Lett. **89**, 037901 (2002).
[113] L. Hofstetter, S. Csonka, J. Nygård, and C. Schönenberger, Cooper pair splitter realized in a two-quantum-dot Y-junction, Nature (London) **461**, 960 (2009).
[114] K. Sato, D. Loss, and Y. Tserkovnyak, Cooper-Pair Injection into Quantum Spin Hall Insulators, Phys. Rev. Lett. **105**, 226401 (2010).
[115] L. Hofstetter, S. Csonka, A. Baumgartner, G. Fülöp, S. d'Hollosy, J. Nygård, and C. Schönenberger, Finite-Bias Cooper Pair Splitting, Phys. Rev. Lett. **107**, 136801 (2011).
[116] K. Sato, D. Loss, and Y. Tserkovnyak, Crossed Andreev reflection in quantum wires with strong spin-orbit interaction, Phys. Rev. B **85**, 235433 (2012).
[117] J. Schindele, A. Baumgartner, and C. Schönenberger, Near-Unity Cooper Pair Splitting Efficiency, Phys. Rev. Lett. **109**, 157002 (2012).
[118] A. Das, Y. Ronen, M. Heiblum, D. Mahalu, A. V. Kretinin, and H. Shtrikman, High-efficiency Cooper pair splitting demonstrated by two-particle conductance resonance and positive noise cross-correlation, Nat. Commun. **3**, 1165 (2012).
[119] G. Fülöp, S. d'Hollosy, A. Baumgartner, P. Makk, V. A. Guzenko, M. H. Madsen, J. Nygård, C. Schönenberger, and S. Csonka, Local electrical tuning of the nonlocal signals in a Cooper pair splitter, Phys. Rev. B **90**, 235412 (2014).
[120] G. Fülöp, F. Domínguez, S. d'Hollosy, A. Baumgartner, P. Makk, M. H. Madsen, V. A. Guzenko, J. Nygård, C. Schönenberger, A. Levy Yeyati, and S. Csonka, Magnetic Field Tuning and Quantum Interference in a Cooper Pair Splitter, Phys. Rev. Lett. **115**, 227003 (2015).
[121] R. S. Deacon, A. Oiwa, J. Sailer, S. Baba, Y. Kanai, K. Shibata, K. Hirakawa, and S. Tarucha, Cooper pair splitting in parallel quantum dot Josephson junctions, Nat. Commun. **6**, 7446 (2015).
[122] S. Baba, C. Jünger, S. Matsuo, A. Baumgartner, Y. Sato, H. Kamata, K. Li, S. Jeppesen, L. Samuelson, H. Q. Xu, C. Schönenberger, and S. Tarucha, Cooper-pair splitting in two parallel InAs nanowires, New J. Phys. **20**, 063021 (2018).
[123] C. Schrade and L. Fu, Parity-Controlled 2π Josephson Effect Mediated by Majorana Kramers Pairs, Phys. Rev. Lett. **120**, 267002 (2018).
[124] X.-J. Liu, C. L. M. Wong, and K. T. Law, Non-Abelian Majorana Doublets in Time-Reversal-Invariant Topological Superconductors, Phys. Rev. X **4**, 021018 (2014).
[125] P. Gao, Y.-P. He, and X.-J. Liu, Symmetry-protected non-Abelian braiding of Majorana Kramers pairs, Phys. Rev. B **94**, 224509 (2016).
[126] C. Schrade and L. Fu, Quantum computing with Majorana Kramers pairs, arXiv:1807.06620.
[127] L. A. Landau, S. Plugge, E. Sela, A. Altland, S. M. Albrecht, and R. Egger, Towards Realistic Implementations of a Majorana Surface Code, Phys. Rev. Lett. **116**, 050501 (2016).
[128] S. Hoffman, C. Schrade, J. Klinovaja, and D. Loss, Universal quantum computation with hybrid spin-Majorana qubits, Phys. Rev. B **94**, 045316 (2016).
[129] T. Karzig, C. Knapp, R. M. Lutchyn, P. Bonderson, M. B. Hastings, C. Nayak, J. Alicea, K. Flensberg, S. Plugge, Y. Oreg, C. M. Marcus, and M. H. Freedman, Scalable designs for quasiparticle-poisoning-protected topological quantum computation with majorana zero modes, Phys. Rev. B **95**, 235305 (2017).